JOURNAL OF MATERIALS SCIENCE 32 (1997) 23–33

Failure of ceramic/fibre-reinforced plastic composites under hypervelocity impact loading

J. JANG, R. PARK,
Department of Chemical Technology, Seoul National University, San 56-1, Shinlimdong Kwanakgu, Seoul, 151-742 Korea

Y. YUN, J. PARK
Agency for Defense Development, Yusung P.O. Box 35, Taejeon, 305-600 Korea

H. KIM*
Department of Ordnance Engineering, Korea Military Academy, P.O. Box 77-2, Gongnuengdong Nowongu, Seoul, 139-799 Korea

The hypervelocity impact limit, V_{50}, of alumina/fibre-reinforced plastic (FRP) target materials was studied with different adhesive layer thicknesses and two kinds of FRP. A high-speed camera was used to analyse the perforation phenomena of target materials. In addition, the dishing and bulging extent of FRP as a rear material were investigated using a digital planimeter from a series of high-speed photographs during the perforation of a projectile. In the case of the same adhesive layer thickness, the target material with more ductile FRP (A type) absorbed more impact energy than that with less ductile FRP (B type). In both target materials, the highest V_{50} was obtained at an adhesive layer thickness of 1.3 mm.

1. Introduction

Recently, high-performance hybrid composites have been used for various applications [1–4]. These hybrid composites offer many advantages, such as excellent specific stiffness and strength, reduced cost, and balanced performance owing to the judicious choice of components [4, 5].

In military applications which are related to personnel body protectors, flak jackets, and protector systems, hybrid composites have been used for the excellent impact resistance and the weight saving of the application material. Although a strict criterion of impact performance and weight saving favours hybrid composites, a design based on materials cost favours ceramics. A protector combining a ceramic face plate with a backing of hybrid composites is a typical example for taking advantage of both materials. In this case, the hybrid composite is attached to the ceramic plate by adhesives [6].

The studies of penetration and perforation of materials have been carried out over many years with the steadily increasing military and civil applications. The dynamic behaviour of high-strength ceramics is of interest in high-pressure shock-wave technologies, and in military applications as components of protector systems [7]. However, most ceramics are very brittle and their fracture occurs by brittle crack propagation up to shattering. There are three possible phases in the penetration of a ceramic protector: (1) shock, in which a high-pressure shock wave followed by a release wave propagates through the ceramic; (2) penetration, in which the projectile penetrates the target by compressive yielding of the target materials in its path; (3) fracture, in which a fracture front propagates into the ceramic ahead of the projectile [8].

The impact energy in hybrid composites is absorbed in two steps: crack initiation and crack propagation. The latter has more effect on impact energy absorption than the former. In the case of crack propagation, the impact response reflects a failure process involving fibre breakage, fibre pull-out, delamination, and debonding [9, 10]. The response of composite materials is impactor-induced surface pressure, internal stress in the composite target caused by the surface pressure, and failure modes in the target caused by the internal stresses. The impact response and failure modes are influenced by the fibre and matrix properties, fibre orientation, stacking sequence, and target thickness [11]. Overall structural deformation by projectile impact is a phenomenon distinct from localized bulging and dishing, which are the displacement of target material at the rear surface of the plate owing to direct pressure from the projectile [6]. The extent of bulging

* Author to whom all correspondence should be addressed.

0022–2461

and dishing in hybrid composites shows the difference of impact energy absorption, and is affected by the adhesive layer thickness and the ductility of fibre-reinforced plastics (FRP).

In this work, the hypervelocity impact limit, V_{50}, of alumina/FRP target materials has been examined with different adhesive layer thicknesses and two kinds of FRP. Perforation phenomena of alumina/FRP were also analysed using a high-speed framing camera, and the deformation of the rear plate was investigated from a series of high-speed photographs during the perforation by the projectile.

2. Experimental procedure

2.1. Materials

The fabrics used for intra-ply hybrid composites were plain types of Kevlar-29 and Spectra-900. Two different intra-ply fabrics were used: the first fabric (A type) was composed of Kevlar in the warp and Spectra in the weft. The second fabric (B type) was composed of Kevlar in the warp, and Kevlar and Spectra alternately in the weft. Kevlar fibre was supplied by Du pont de Nemours and Co. Inc., in the form of a 4800 denier, 480 filament yarn, and Spectra fibre was provided by Allied Signal Co. in the form of a 3000 denier, 300 filament yarn. The used matrix resin was styrene-based XSR-10 vinylester resin, supplied by National Synthesis Co. Benzoyl peroxide (2 wt%) was added to the matrix resin as a reaction initiator.

The ceramic used as a face plate was alumina, supplied by Daehan Joongsuk Co. The hybrid composites were attached to the alumina plate with epoxy adhesive B1 and B2 provided by B.F. Goodrich Co., and the adhesive layer thicknesses were 0.8, 1.3 and 2.3 mm.

The physical properties of alumina and hybrid composites used in this study are given in Table I.

TABLE I Physical properties of alumina and hybrid composites

Materials		Density ($g\,cm^{-3}$)	Thickness (mm)	Areal density ($g\,cm^{-2}$)
Al_2O_3		3.38	8.19	2.77
Kevlar-Spectra/Vinylester	A type (50:50)	1.18	6.50	0.77
	B type (75:25)	1.30	6.50	0.85

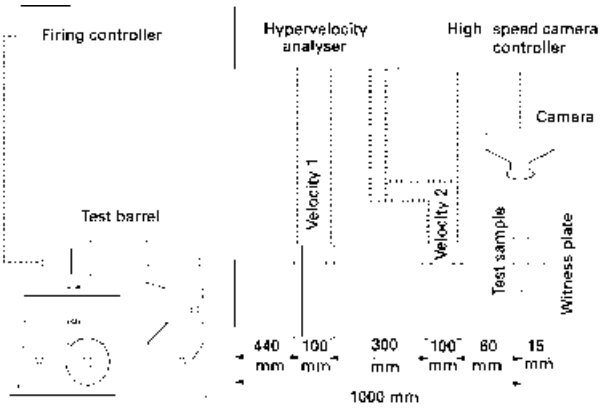

Figure 1 A schematic diagram of the hypervelocity impact apparatus for testing alumina/FRP target materials.

2.2. Hypervelocity impact testing

In hypervelocity impact tests, measurements were mainly concerned with the determination of the projectile impact velocities. A schematic diagram of the hypervelocity impact apparatus used in this study is shown in Fig. 1. It consists of the following parts: (a) an impact rifle, of 7.62 mm calibre, firing standard lead bullets; (b) a long steel test stand, used to support individual components of the testing arrangement; (c) frames used for velocity measurement (for each projectile, four frames were prepared, two of which were used for the measurement of initial impact velocity, and the other two for the measurement of later impact velocities before the target; each frame was connected to an electronic counter to measure the projectile travel time in microseconds); (d) square target plates and witness plate (the size of the alumina face plate was 15 cm × 15 cm, and the composite rear plate 30 cm × 30 cm; a witness plate was located behind the target, and complete penetration was defined as perforation of both target and witness plate); (e) a high-speed camera located on the lateral side of the target material to investigate perforation phenomena.

Test results were reported as hypervelocity impact limit, V_{50}, at which theoretically 50% of the travelling projectiles penetrate the target and the other travelling projectiles are stopped. The exact methodology of calculating the hypervelocity impact limit is described in MIL-STD-662. In the simplest case, a V_{50} is determined by averaging four projectile-striking velocities that include the two lowest velocities which result in a complete penetration (CP), and the two highest velocities that result in a partial penetration (PP). A spread of $16\,m\,s^{-1}$ or less is required between the lowest velocity for PP and the highest velocity for CP. In practice, time and economic constraints limit the quantity of data obtained. Therefore, we accepted data obtained unless a large discrepancy from the above conditions existed.

The projectile-striking velocity according to propellant weight is represented in Fig. 2, and the required striking velocity was achieved through a change of propellant weight.

2.3. Analysis of perforation phenomena

Perforation phenomena were analysed using the high-speed camera during the penetration of target materials. The dishing and bulging extent of hybrid composites, a rear plate of target material, with change of time, were measured from the displacement difference from before and after deformation by a digital planimeter.

3. Results and discussion

3.1. The hypervelocity impact limit

In designing a protector system based on ceramic/FRP composites, the foremost concern is the prevention

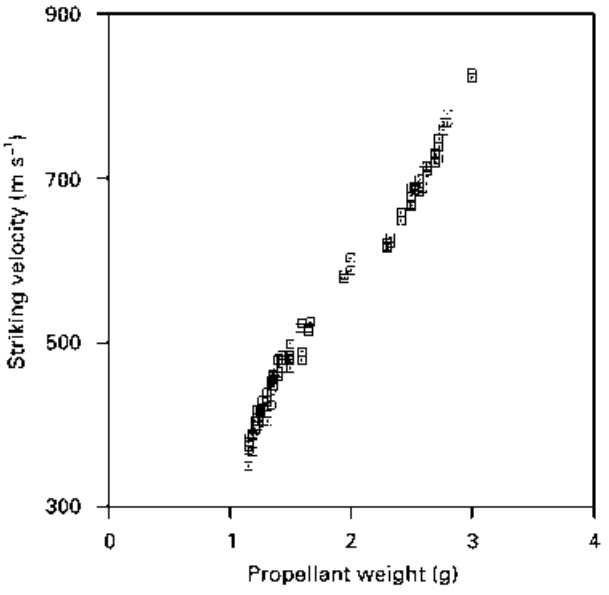

Figure 2 The projectile-striking velocity according to propellant weight in 7.62 mm AP.

of projectile penetration. As a result, the most important parameter in evaluating the impact resistance of ceramic/FRP is the hypervelocity impact limit below which no penetration occurs. Table II summarizes the hypervelocity impact limit, V_{50}, of alumina/FRP target materials in the case of using two kinds of rear plate with different adhesive layer thicknesses. In each case, CP and PP of target materials were determined after impact and the effective selection was made to estimate the V_{50} by the criterion represented in MIL-STD-662. Effective data selection for V_{50} was made through a CP and a PP to reduce velocity spread between selected CP and PP. Each target material showed the highest V_{50} at an adhesive layer thickness of 1.3 mm. In addition, for the same adhesive layer thickness, target material with A type composite shows a better impact performance than that with B type composite. High-strength polyethylene fibre with a very ductile property absorbs more impact energy through fibre pull-out rather than fibre breakage, while aramid fibre, less ductile compared with high-strength polyethylene fibre, absorbs less impact energy owing to fibre breakage by low elongation [12–14]. As a result of these fibre-impact properties, Spectra-reinforced composites show a good impact property owing to fibre pull-out and delamination, which result in bulging and dishing of the composite over a wide range after impact. Therefore, the target material with A type hybrid composite, which contains 50% Spectra by volume, shows a better impact performance compared with target material containing B type composite with 25% Spectra by volume.

3.2. The effect of FRP type

Significant differences in the impact performance were observed between target material with A type FRP and target material with B type FRP. A high-speed camera was used to analyse the perforation phenomena of target materials and the deformation extent of FRP which was related to penetration resistance as well as impact energy absorption. Fig. 3 shows a series of high-speed photographs of AP projectile impacting alumina/FRP (B type) target material with an adhesive layer thickness of 2.3 mm. The high-speed camera used in this study can take data at a recording rate of 35 000 frames s^{-1} and its resolution time is 28.6 μs. Fig. 3a shows a photograph of a projectile before impact, and Fig. 3b and c demonstrate alumina shattering of a face material and the onset of the dishing and bulging phenomenon in the rear hybrid composite. Alumina shattering, dishing, and bulging appear to a larger extent with increasing time. Fig. 3e shows the onset of perforation of the rear composite, and the perfect perforation is shown in Fig. 3i–l through fibre breakage and scattering of the broken fibre. Impact energy is seen to be absorbed in three regions (alumina, adhesive layer, and hybrid composite) from the series of photographs represented above. Alumina shattering is shown by radial cracks and lateral crack propagation owing to compressive stress during the impact. The adhesive layer plays a role in transferring the compressive stress applied to the alumina, to the rear material, so that the flexibility or rigidity of the adhesive layer has an effect on the impact energy absorption of the rear material as well as the adhesive layer. In addition, the rear hybrid composite absorbs impact energy through dishing and bulging, which are the structural deformation of FRP by fibre pull-out and delamination.

The fracture behaviour of the impact and rear surfaces of alumina/FRP (B type) target material with an adhesive layer of thickness 2.3 mm is shown in Fig. 4. No alumina nor adhesive layer remain on the impact surface. This is due to alumina shattering and debonding at the interface between the adhesive layer and the FRP, which absorb the impact energy of the projectile. The rear surface shows the behaviour of linear fibre breakage resulting from the low elongation of Kevlar and the high ductility of Spectra. While fibre stretching and pull-out occur in Spectra, fibre breakage occurs in Kevlar, which results in linear fracture in the longitudinal direction of Spectra.

Fig. 5 indicates the dishing and bulging extent of the rear material in alumina/FRP (B type) target material from the deformation degree in Fig. 3b–g. In the initial impact step from Fig. 5b to d, the deformation in the transverse direction of a projectile by the dishing phenomenon results from debonding at the fibre–matrix interface due to the impact energy splitting in the longitudinal direction of the fibre. The bulging, which is the deformation in the longitudinal direction of a projectile, is caused by fibre pull-out and delamination. Fig. 5e indicates the onset of FRP perforation, and the bulging extent increases largely with a slight increase of dishing in the later impact step. In addition, the deformation depth around a projectile increases largely by fibre pull-out and stretching in a narrow region.

A series of high-speed photographs of AP projectile impacting alumina/FRP (A type) target material with an adhesive layer thickness of 2.3 mm is shown in Fig. 6. Fig. 6b and c indicate the onset of alumina

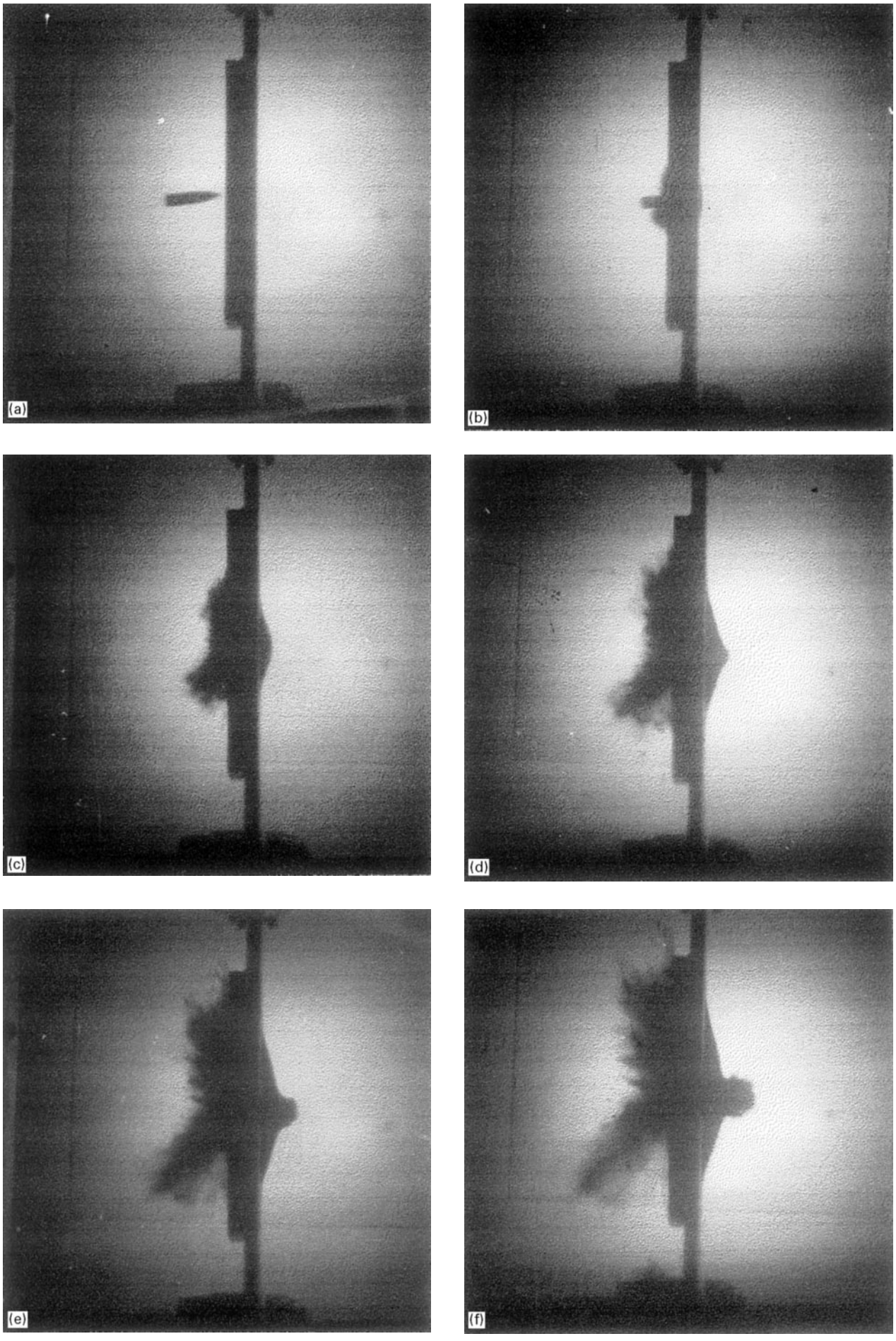

Figure 3 A series of high-speed photographs of alumina/FRP (B type) target material with an adhesive layer thickness of 2.3 mm: the projectile-striking velocity was 729 $m\,s^{-1}$ (a) 0 μs, (b) 28.6 μs, (c) 57.2 μs, (d) 85.8 μs, (e) 114.4 μs, (f) 143.0 μs, (g) 171.6 μs, (h) 200.2 μs, (i) 228.8 μs, (j) 257.4 μs, (k) 286.0 μs, (l) 314.6 μs.

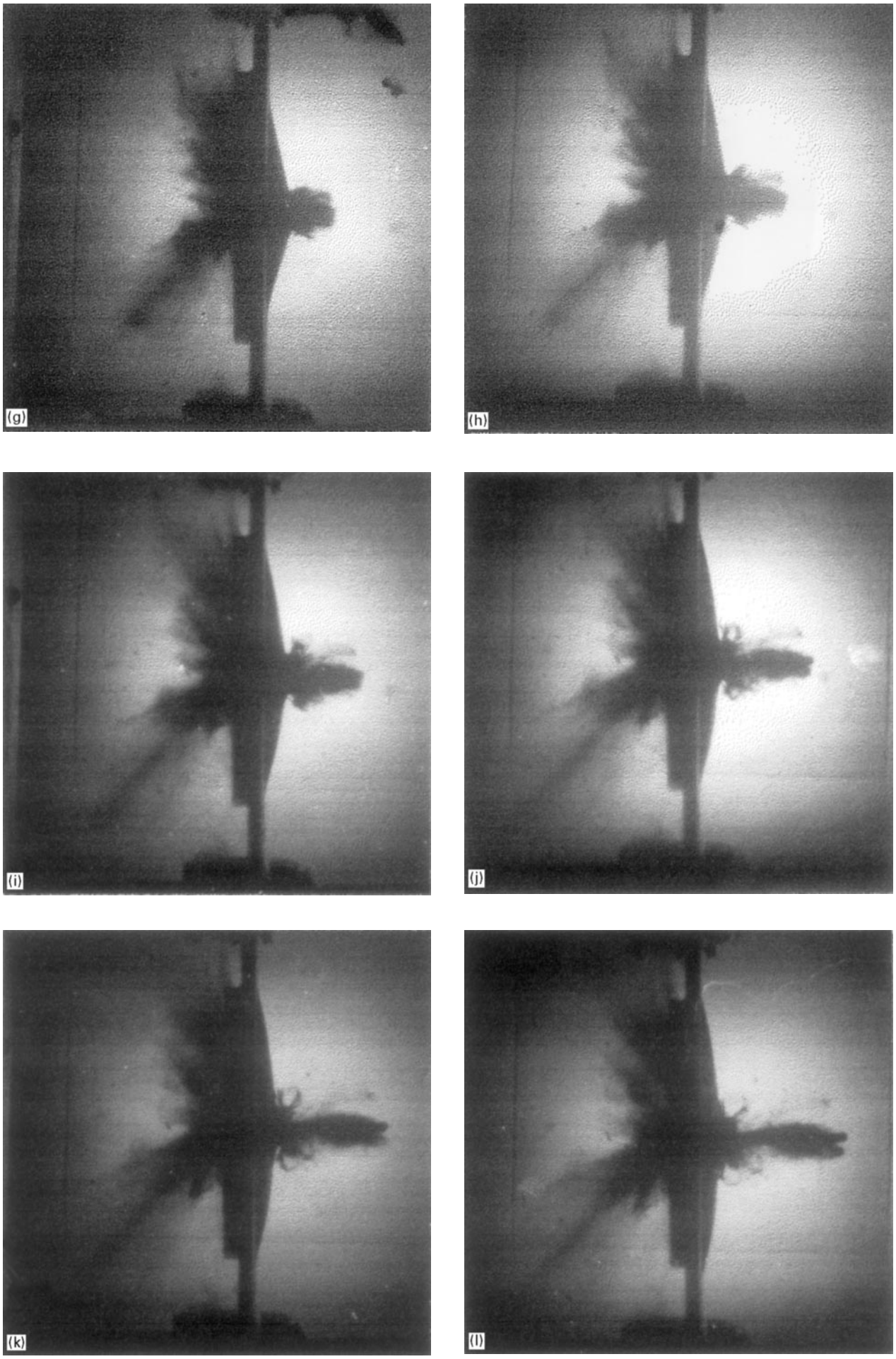

Figure 3 (Continued).

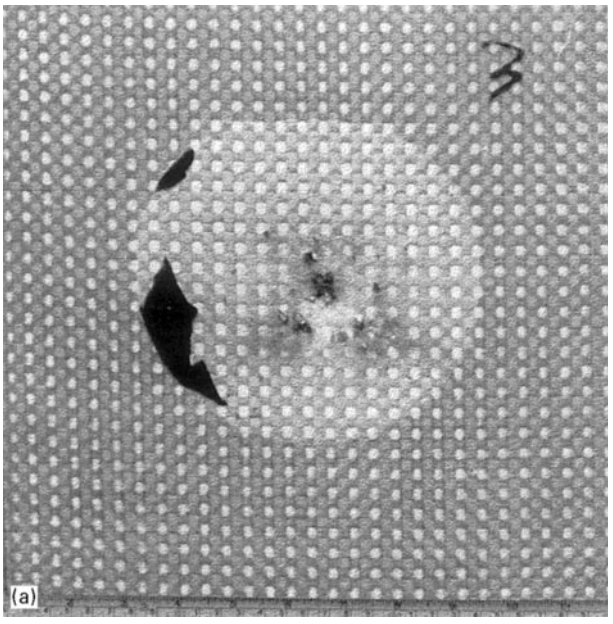

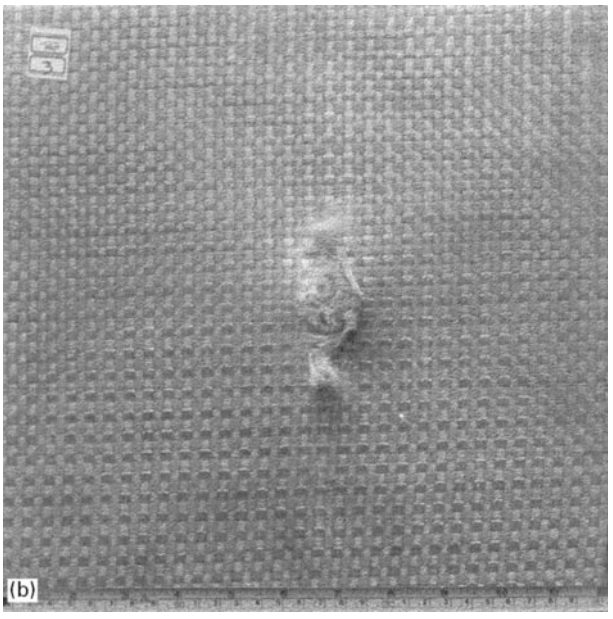

Figure 4 The fracture behaviour in (a) the impact surface and (b) the rear surface of alumina/FRP (B type) target material with an adhesive layer thickness of 2.3 mm.

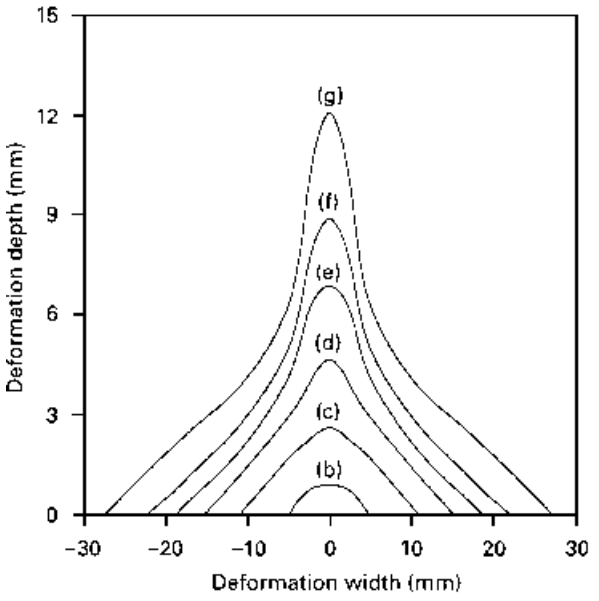

Figure 5 The dishing and bulging extent of the rear material in alumina/FRP (B type) target material with an adhesive layer thickness of 2.3 mm.

shattering and FRP deformation, and FRP perforation is represented in Fig. 6e–1. In the initial impact step from Fig. 6b to g, a lesser dishing extent and a similar bulging extent are shown compared with Fig. 3. However, in the later impact step, the bulging extent increases steadily with a slight increase of dishing, while in the case of Fig. 3, the dishing and bulging extents formed in the initial step are almost retained constantly throughout the overall steps. The difference between the two cases results from the dissimilar ductility of the hybrid composites used as rear materials. The target material with a more ductile property can resist the applied impact better, so that the bulging extent increases during perforation with time. Type A hybrid composite with more Spectra exhibits a more ductile property, and indicates a larger bulging degree with increasing time, from Figs 3 and 6.

Fig. 7 indicates the dishing and bulging extent of the rear material in alumina/FRP(A type) target material from the deformation degree in Fig. 6c–g. The dishing and bulging extent increase with increasing test time, and the onset of FRP perforation is shown in Fig. 7e. In the initial impact step from Fig. 7c to g, the dishing extent is less, and the bulging extent represents the almost similar form compared with Fig. 5. This result corresponds to the photographs in Figs 3 and 6. Therefore, the target material with a more ductile property absorbs more impact energy through a remarkable increase of dishing and bulging in the later impact step. As shown in Figs 3 and 5, however, less ductile target material absorbs less impact energy by a slight increase of the bulging extent in the later impact step.

Fig. 8 shows the deformation area of the rear material in alumina/FRP target material calculated using a digital planimeter from the dishing and bulging extent in the photographs of Figs 3 and 6. The adhesive layer thickness between the alumina and FRP was 2.3 mm in both cases. Therefore, the hypervelocity impact limit in each case depends on the dishing and bulging extents of FRP, which indicate the degree of impact energy absorption through structural deformation during the impact. The larger the deformation area, the more impact energy is absorbed. In the initial impact step, the deformation area indicates the slightly higher value in B type FRP, which contains 25% Spectra by volume and 75% Kevlar by volume. This is due to the larger dishing extent in the initial impact step. In the later impact step, the deformation area shows the higher value in A type FRP, which contains 50% Spectra by volume. The more ductile target material resists impact successively, so that it shows a wider deformation area by a remarkable increase of bulging extent with time. However, B type FRP shows a narrower deformation area due to the brittle property in the later impact step with a slight increase of bulging extent formed initially.

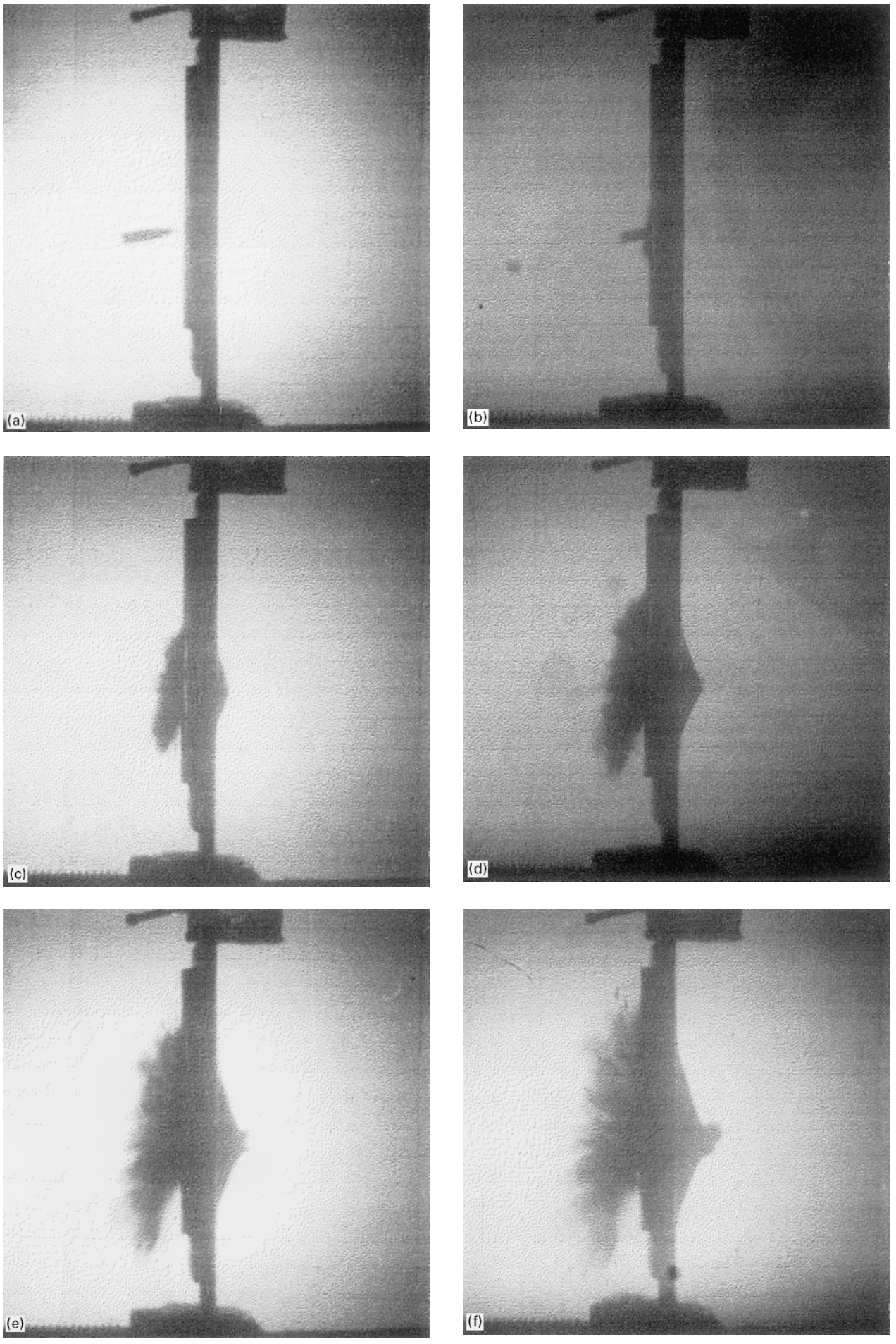

Figure 6 A series of high-speed photographs of alumina/FRP (A type) target material with an adhesive layer thickness of 2.3 mm: the projectile-striking velocity was 725 $m\,s^{-1}$ (a) 0 μs, (b) 28.6 μs, (c) 57.2 μs, (d) 85.8 μs, (e) 114.4 μs, (f) 143.0 μs, (g) 171.6 μs, (h) 200.2 μs, (i) 228.8 μs, (j) 257.4 μs, (k) 286.0 μs, (l) 314.6 μs.

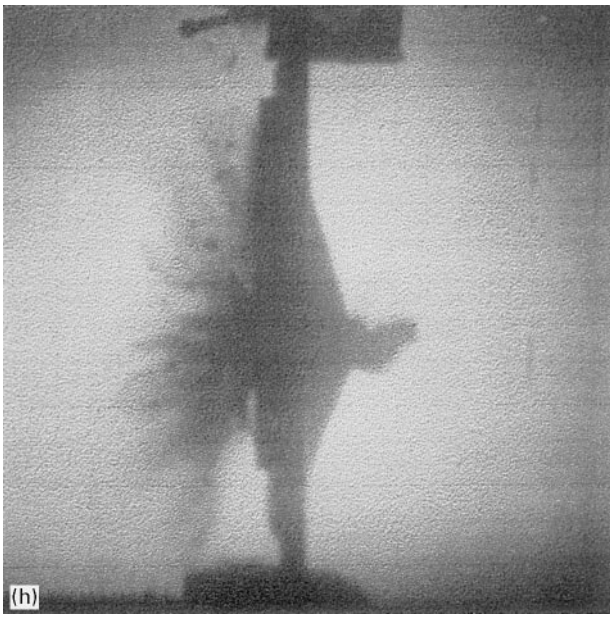

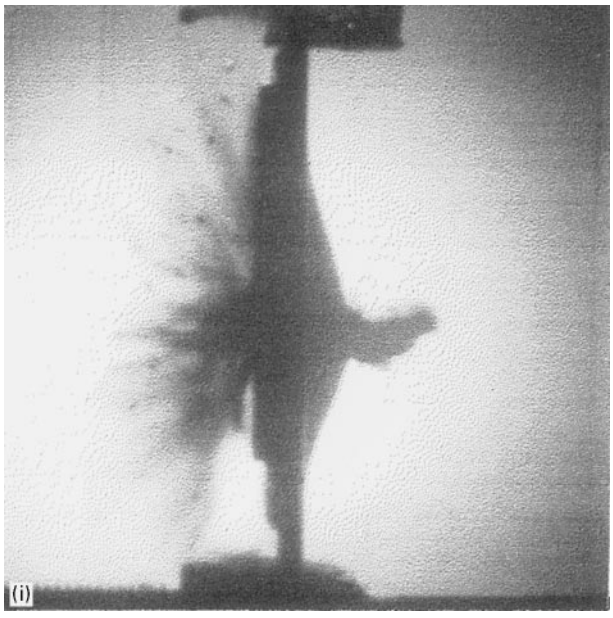

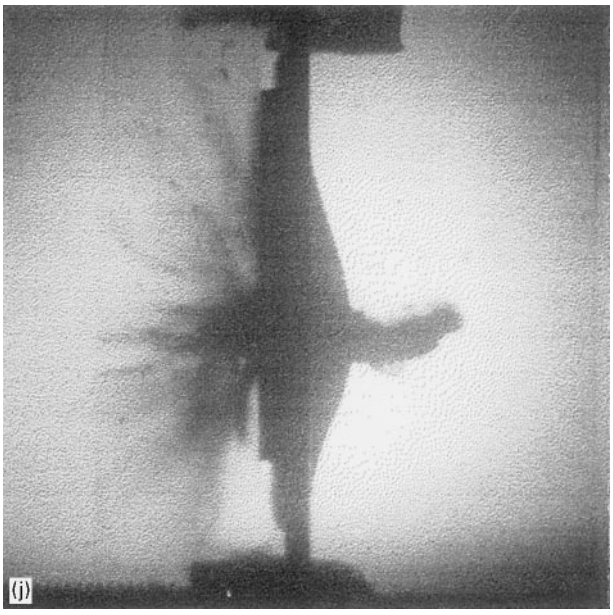

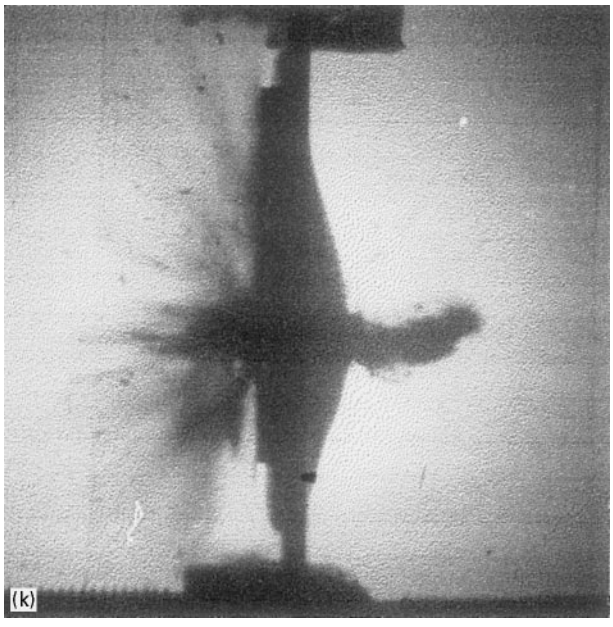

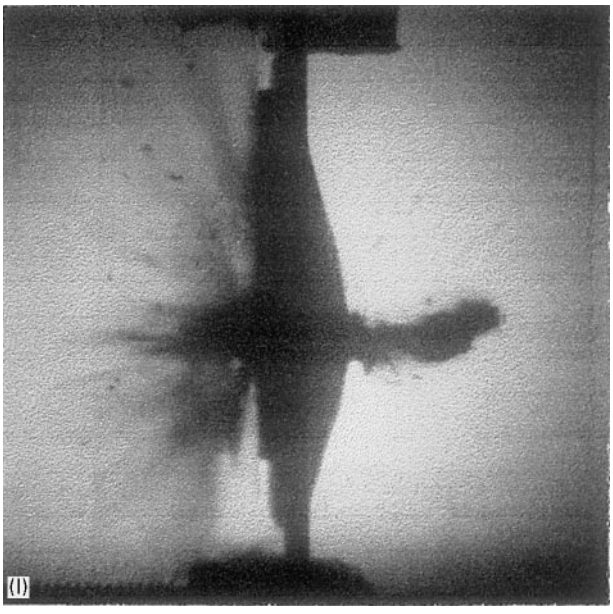

Figure 6 (Continued).

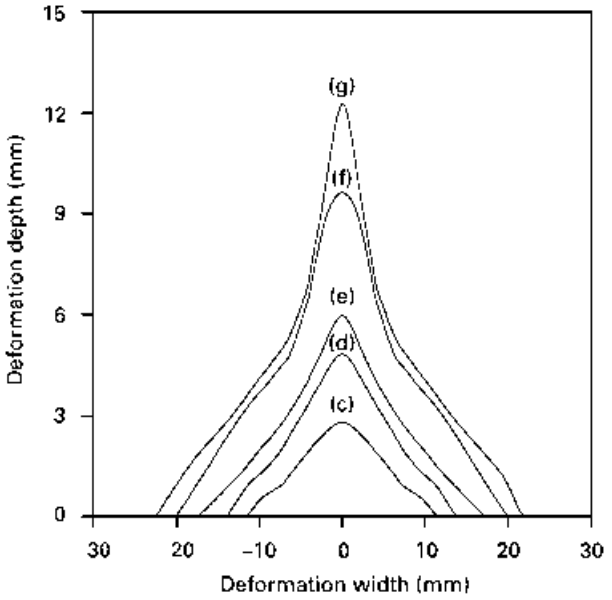

Figure 7 The dishing and bulging extent of the rear material in alumina/FRP (A type) target material with an adhesive layer thickness of 2.3 mm.

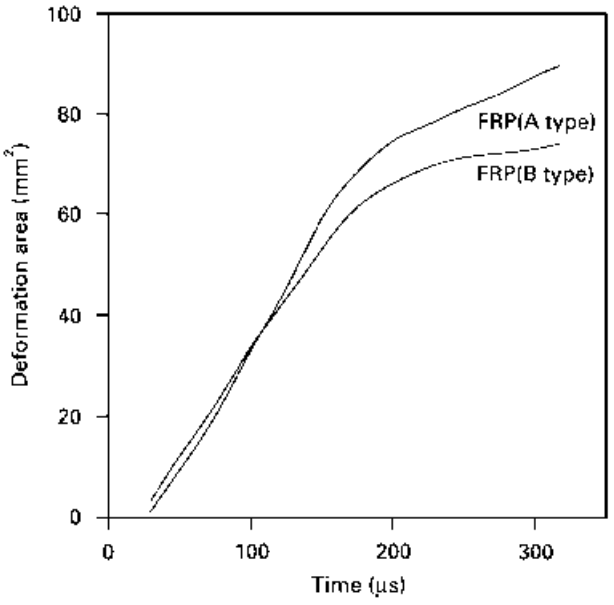

Figure 8 The deformation area of FRP in the alumina/FRP target material according to perforation time with an adhesive layer thickness of 2.3 mm.

3.3. The effect of adhesive layer thickness

The highest V_{50} was found at an adhesive layer thickness of 1.3 mm in both target materials, as shown in Table II. Owing to the similar trend in the two cases, the fracture behaviour of the target material with A type FRP will be shown. The fracture behaviour of the impact and rear surfaces of alumina/FRP (A type) target material with different adhesive layer thicknesses is shown in Fig. 9. In the case of an adhesive layer thickness of 1.3 mm, no alumina nor adhesive layer remains in the impact surface. Much impact energy is absorbed by the perfect interfacial debonding between the adhesive layer and FRP, and the deformation through the overall FRP is observed in the rear surface and side view. However, in the case of adhesive layer thicknesses of 0.8 and 2.3 mm, the amounts of alumina and adhesive layer remain slight

TABLE II The hypervelocity impact limit, V_{50}, of alumina/FRP target materials against 7.62 mm AP projectile

Materials	Adhesive layer thickness (mm)	Hypervelocity impact limit, V_{50}, ($m\,s^{-1}$)
Alumina/FRP (A type)	0.8	720.0
	1.3	832.8
	2.3	722.5
Alumina/FRP (B type)	0.8	693.4
	1.3	780.2
	2.3	699.6

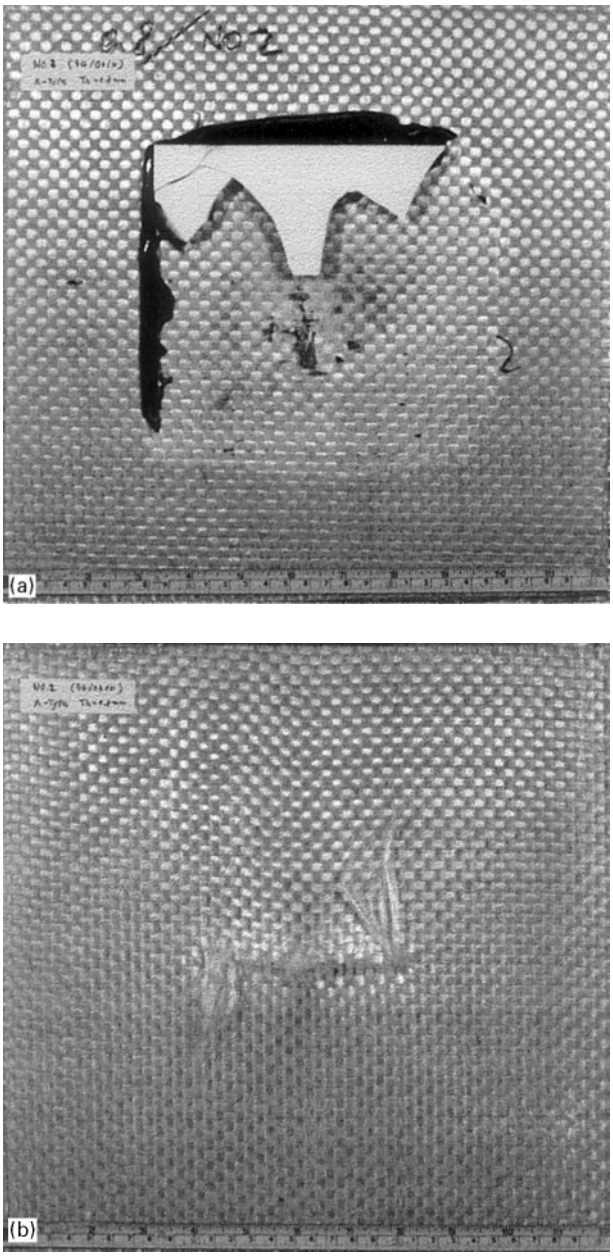

Figure 9 The fracture behaviour in (a, c, f) the impact, (b, d, g) the rear and (c) side surfaces of alumina/FRP (A type) target material with different adhesive layer thicknesses: (a, b, c) 0.8 mm, (e, d, f) 1.3 mm, (g) 2.3 mm.

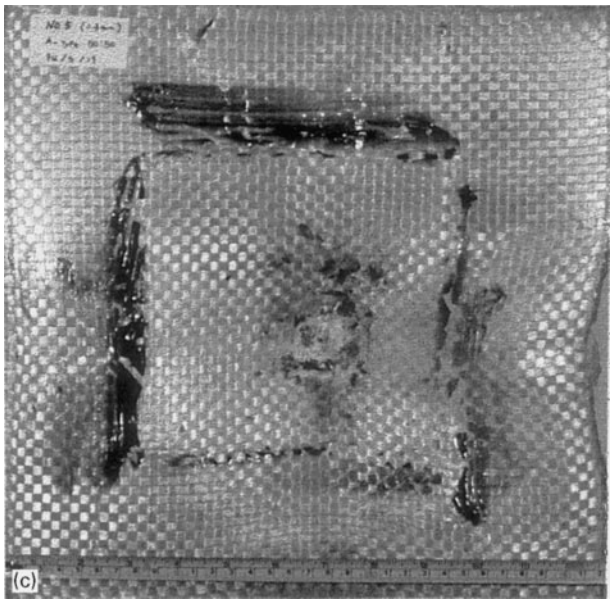

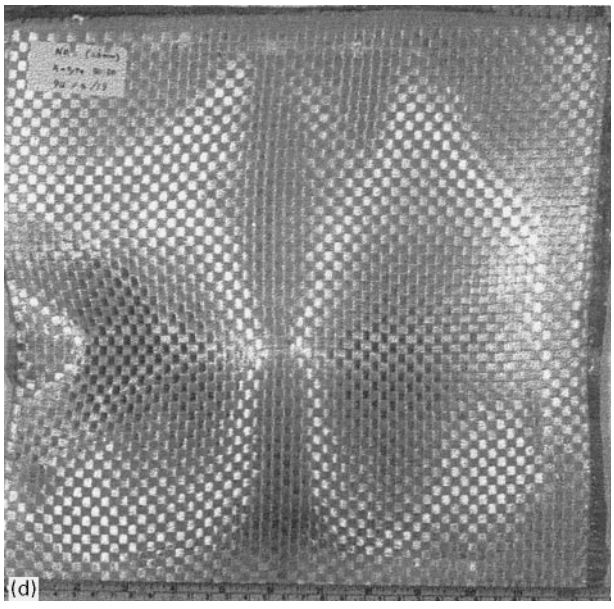

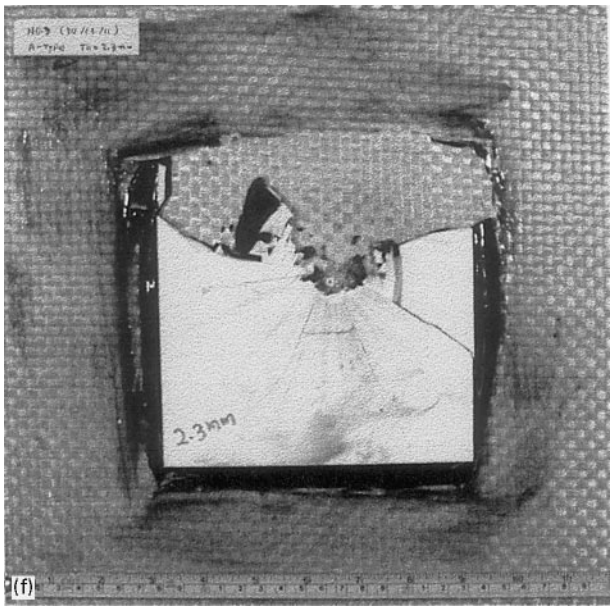

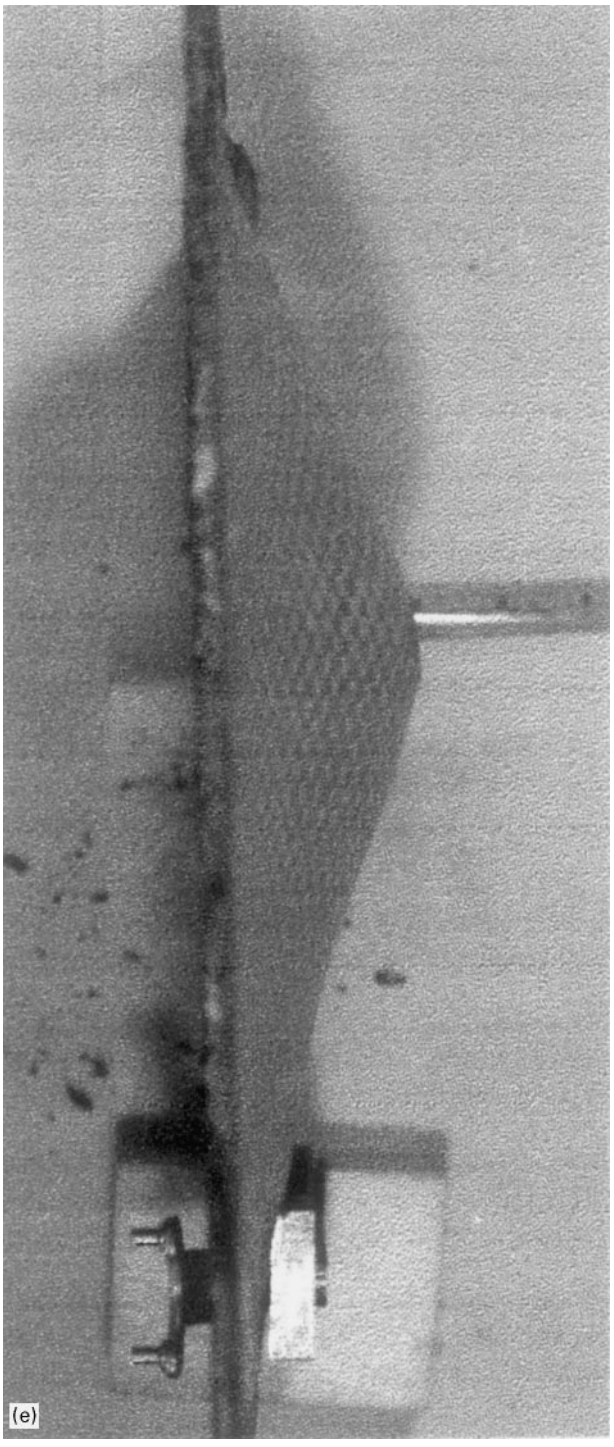

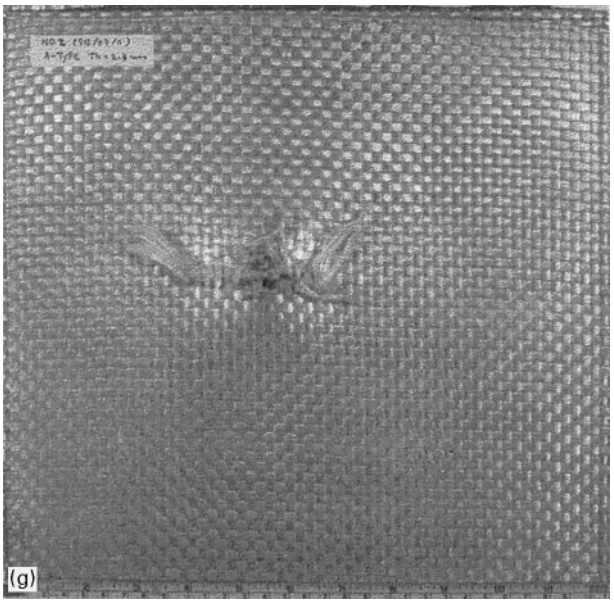

Figure 9 (Continued).

in the impact surface. Interfacial debonding between the adhesive layer and FRP occurs in narrower region, and this results in a decrease of the deformation in FRP. The rear surface shows the behaviour of linear fibre breakage which results from the low elongation of Kevlar and the high ductility of Spectra, as shown in Fig. 4. Adhesive layer thickness has an effect on the degree of interfacial debonding, the deformation of FRP, and the final impact performance of alumina/FRP. Adhesive layer thickness, flexibility or rigidity of the adhesive layer, affects the location where the failure initiates [11]. For flexible thin thickness, the impact damage initiates on the bottom surface and is governed by plate bending stress. As the thickness of the adhesive layer increases, the plate bending stress becomes small and impact damage initiates on the impact surface by local contact stress. Therefore, in the case of adhesive layer thicknesses of 0.8 and 2.3 mm, the failure of the adhesive layer caused by compressive stress applied to the alumina occurs on the bottom surface and the local contact surface of adhesive layer, respectively. This results in the local interfacial debonding between the adhesive layer and the FRP. In addition, this causes a decrease of the deformation area in the FRP and a worse impact performance. However, in the case of an adhesive layer thickness of 1.3 mm, the failure of the adhesive layer occurs in the overall region of the adhesive layer, not in the bottom surface and the local contact surface. This results in perfect interfacial debonding and the overall deformation of FRP, which cause the better impact performance.

4. Conclusion

The hypervelocity impact limit, V_{50}, of alumina/FRP was studied with different adhesive layer thicknesses and two kinds of FRP. The impact energy of the target materials was found to be absorbed in three regions, alumina, adhesive layer, and hybrid composite, from a series of photographs. In the case of the same adhesive layer thickness, the target material with the more ductile FRP (A type) absorbed more impact energy through a large increase of dishing and bulging in the later impact step. However, the target material with the less ductile FRP (B type) absorbed less impact energy by a slight increase of the bulging extent in the later impact step. Adhesive layer thickness, flexibility or rigidity of the adhesive layer, affected the interfacial debonding between the adhesive layer and the FRP, the deformation extent in the FRP, and the impact performance of alumina/FRP. In both target materials, the highest V_{50} was found at an adhesive layer thickness of 1.3 mm.

References

1. Y. QIU and P. SCHWARTZ, *Compos. Sci. Technol.* **47** (1993) 303.
2. *Idem*, *ibid.* **47** (1993) 289.
3. G. PERNANDO, R. F. DICKSON, T. ADAM, H. REITER and B. HARRIS, *J. Mater. Sci.* **23** (1988) 3732.
4. N. L. HANCOX, "Fiber Composite Hybrid Materials" (Applied Science, London, 1981).
5. C. W. CAMACHO, C. L. TUCKER III, S. YALVAC and R. L. McGEE, *Polym. Compos.* **11** (1990) 229.
6. J. MORTON, "Structural Impact and Crashworthiness" (Elsevier Applied Science, London, 1984).
7. I. GILATH, S. ELIEZER and Y. GAZIT, *J. Mater. Sci.* **26** (1991) 2023.
8. S. J. BLESS, Z. ROSENBERG and B. YOON, in "Proceedings of the 1986 Symposium on Hypervelocity Impact", Texas, October 1986, edited by C. E. Anderson (Pergamon Press, Oxford, 1987).
9. R. H. ZEE, C. J. WANG, A. MOUNT, B. Z. JANG and C. Y. HSIEH, *Polym. Compos.* **12** (1991) 196.
10. S. M. LEE, *J. Compos. Mater.* **20** (1986) 185.
11. J. A. ZUKAS, T. NICHOLAS, H. F. SWIFT, L. B GRESZCZUK and D. R. CURRAN, "Impact Dynamics" (Wiley, New York, 1982).
12. B. L. LEE, J. W. SONG and J. E. WARD, *J. Compos. Mater.* **28** (1994) 1203.
13. N. H. SADIZESKY and I. M. WARD, *Compos. Sci. Technol.* **26** (1986) 199.
14. B. Z. JANG, L. C. CHEN, C. Z. WANG, H. T. LIN and R. H. ZEE, *Compos. Sci. Technol.* **34** (1989) 305.

Received 30 August 1995
and accepted 21 May 1996